Observation of the Cumbre Vieja volcano plume above the Observatorio del Roque de los Muchachos with the Barcelona Raman LIDAR

M Živec[1], O Ballester[2], O Blanch[2], J Boix[2], P G Calisse[3], A Campoy Ordaz[4], M Doro[5], L Font[4], R Garcia[2], M Gaug[4], R Grau[2], M Martinez[2], D Roman[2], S Stanič[1], S Ubach Ramirez[4], M Zavrtanik[1,6]

[1]University of Nova Gorica, Vipavska 13, 5000 Nova Gorica, Slovenia
[2]Institut de Fisica d'Altes Energies (IFAE), The Barcelona Institute of Science and Technology, Campus UAB, 08193 Bellaterra (Barcelona), Spain
[3]Cherenkov Telescope Array Observatory gGmbH (CTAO gGmbH), Saupfercheckweg 1, 69117 Heidelberg, Germany
[4]Universitat Autònoma de Barcelona and Centre d'Estudis i Recerca Espacial, CERES (IEEC-UAB), 08193 Bellaterra, Spain
[5]Università degli Studi di Padova and INFN Sezione di Padova, Via Marzolo 8, 35131 Padova, Italy
[6]Jožef Stefan Institute, Jamova 39, 1000 Ljubljana, Slovenia

E-mail: miha.zivec@ung.si

Abstract. The Cherenkov Telescope Array Observatory (CTAO), currently under construction, is the next-generation very-high-energy gamma-ray observatory, providing the coverage for photons in the energy range 20 GeV to 300 TeV. CTAO will increase detection sensitivity in the 100 GeV to 10 TeV range by a factor of $5 - 10$ with respect to present experiments. CTAO retrieves the properties of very-high-energy gamma-rays by measuring Cherenkov light emitted by atmospheric showers of secondary particles that incident gamma rays produce in upper layers of the atmosphere. The key for reaching the required energy measurement accuracy is a precise knowledge of the atmospheric transmittance for Cherenkov light, which can be obtained using a dedicated Raman LIDAR. The device should operate at 355 nm (near the maximum of Cherenkov light spectrum) and have the capability of taking data at specific azimuth and zenith angles up to distances of 30 km, so that atmospheric transmission along all possible air-shower directions can be determined. The *Barcelona Raman LIDAR* (BRL) is the official CTAO Pathfinder prototype, developed for atmospheric characterization of the Northern CTAO Site at the Observatorio del Roque de los Muchachos (ORM) on the Canary island of La Palma. BRL was deployed at ORM for extensive on-field tests between February 2021 and May 2022. We report on the commissioning results, including the remote operation capabilities of the system and its contribution to the understanding of atmospheric phenomena during its deployment period. In particular, we report on the properties of the volcanic plume from the eruption of the Cumbre Vieja volcano on 22 September 2021.

1. Introduction

Most events that affect atmospheric optical properties occur in the troposphere and tropopause. At the Cherenkov Telescope Array Observatory (CTAO) northern site, located at the Observatorio del Roque de los Muchachos (ORM) on the Canary island of La Palma, with approximate latitude of 28° North the troposphere thickness varies between 6 km and 18 km [1]. The atmospheric molecular content varies slowly [2], usually on time scales of the order of days to months, while aerosol concentrations change much quicker, on the order of hours. They are most abundant in the lowest part of the troposphere, the planetary boundary layer (PBL), which experiences a regular daily cycle of its properties due to solar irradiation. The PBL can be between few hundred meters to several kilometers thick at the CTAO-N site [3] and is directly influenced by interactions of the atmosphere with the Earth's surface [4] and experiences turbulent transport of moisture and aerosols. Large aerosol densities in the PBL strongly influence light travel due to absorption and scattering. Even though the PBL almost disappears at night, it may leave some residual layer that interferes with the Cherenkov light, which is emitted by atmospheric airshowers of secondary charged particles, arising from the interaction of very high energy cosmic photons with the atmosphere [5].

The main systematic uncertainty in the measurement of very-high energy cosmic gamma-ray properties comes from the need to use the atmosphere as a calorimeter [6]. Due to the different disturbances and changes in aerosol type and loading, this dependence also varies in time. Photon loss is determined by absorption in the atmosphere and scattering out of Imaging Atmospheric Cherenkov Telescopes (IACTs) field of view. To correctly calibrate IACT measurements, constant monitoring of aerosol extinction is required. For this the best suited tool is a LIDAR working in the same wavelength range as IACTs [7].

Elastic LIDARs are the simplest LIDAR class, which only uses elastically backscattered light. The power measurement of this system depends on two unknown physical quantities (the total optical and backscattered coefficient), meaning an assumption is needed. As a result multiple assumptions need to be made, or boundary calibrations introduced, limiting the uncertainty of the height-dependent atmospheric extinction to about 20% for the general case and $\lesssim$5% for the CTAO-N site and a carefully absolutely calibrated LIDAR [3]. Introducing a Raman channel to the system allows simultaneous and independent measurements of the extinction and backscattering coefficient. The assumptions are not needed anymore, and the uncertainty of retrieved atmospheric extinction can be reduced below 5% if multiple Raman lines are used.

2. CTAO-N Raman LIDAR Pathfinder

The Barcelona Raman LIDAR (BRL) [8, 9] is a Raman LIDAR providing scanning capabilities in azimuth and zenith and can be operated remotely. It was awarded the status of a CTAO Raman LIDAR Pathfinder in 2019, implying its potential for future permanent inclusion into the CTAO North observatory. The BRL has a 1.8 m diameter primary mirror with an f-number of 1, protected by four petals (Fig. 1), to prevent any possible direct impact by sunlight, mechanical damage and deposition of dust on its surface. The mirror was produced for the CLUE experiment (Cherenkov Light Ultraviolet Experiment) in Padova [10] with a slumping technique developed at CERN [11, 12]. A final realuminization, this time including protective coating, was performed in Milan, Italy (*ZAOT s.r.l.*) at the end of 2020, before shipping the LIDAR to La Palma. In addition to the primary mirror, the LIDAR system incorporates two guiding mirrors (Fig. 1f) that are used for guiding the laser beam to align with the optical axis of the primary mirror in a co-axial configuration. This allows to reduce the complete overlap distance of the laser beam and the field of view of the receiver. The dichroic guiding mirrors reflect light at an angle of $61.1 \pm 0.3°$ and have very high reflectivity at the wavelengths 355 nm and 532 nm, while other wavelengths (including the 1064 nm laser wavelengh) are suppressed. In order to further increase the dynamic range of the system, special custom-designed near-range optics are used. While the

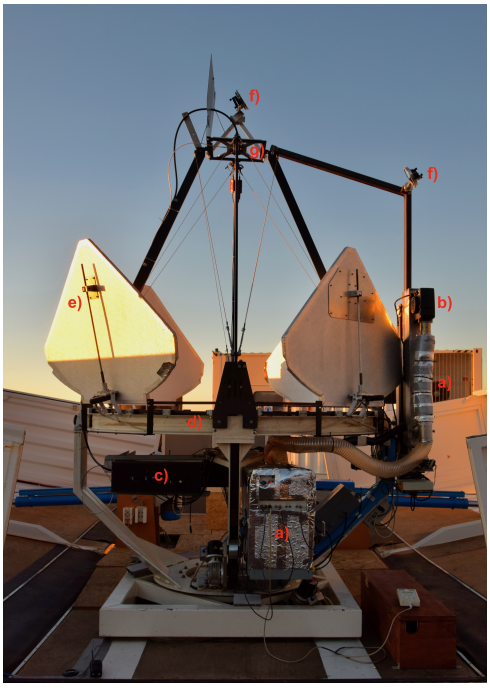

Figure 1: The Barcelona Raman LIDAR deployed for operation at the LST-1 site, Roque de los Muchachos Observatory, La Palma in August 2021. The following LIDAR components are highlighted: (a) laser power and laser head, (b) heater for laser operation under cold ambient temperature conditions, (c) polychromator, (d) main mirror, (e) petals, (f) guiding dichroic mirrors for the transmitter and (g) shutter for the optic fiber.

main LIDAR optics provide access to distance ranges greater than ∼150 m, the near-range optics cover 20 m to ≳200 m distance in the LIDARs field of view. At present, the near-range optics can be used only for the elastic scattering (532 nm) channel. As light source a QUANTEL Brilliant Nd:YAG 1064 nm was used, providing pulses at 10 Hz with a base wavelength of 1064 nm. Second (532 nm) and third (355 nm) harmonics are included, respectively, providing 160 mJ and 70 mJ energy per pulse. The laser head with both harmonic generators is placed in a compact module located on the laser arm (Fig. 1a and b) and moves together with the receiving telescope. The laser system incorporates a cooling and heating unit, providing optimal temperature range to minimize beam quality variations. Both units are mounted in such a way that they move with the receiver and the laser arm and do not limit the LIDAR movement. Elastic and Raman backscattered signals are separated using a custom designed polychromator with four read-out channels [15]. Two of them are used for elastically backscattered light at wavelengths of 355 nm and 532 nm, and two for the Nitrogen Raman signal at wavelengths of 387 nm and 607 nm. The BRL itself is enclosed in a standard (20 ft long) shipping container that protects the device and the accompanying instrumentation from environmental influences. When the LIDAR is in operation, the container is open, which is achieved by two linear actuators. Inside, the receiver and the transmitter are placed on a custom-made alt-azimuth mount, that allows zenith and azimuth angle movements.

From February 2021 on, the BRL was undergoing extensive tests at the CTAO-N site, close to the designated site of the future CTAO-N Raman LIDAR next to the LST-1 telescope [16] during 15 months. During this time the performance of all LIDAR subsystems including full remote operation since September 2021 was verified. The observed problems were addressed and will provide feedback for the final upgrade of the system.

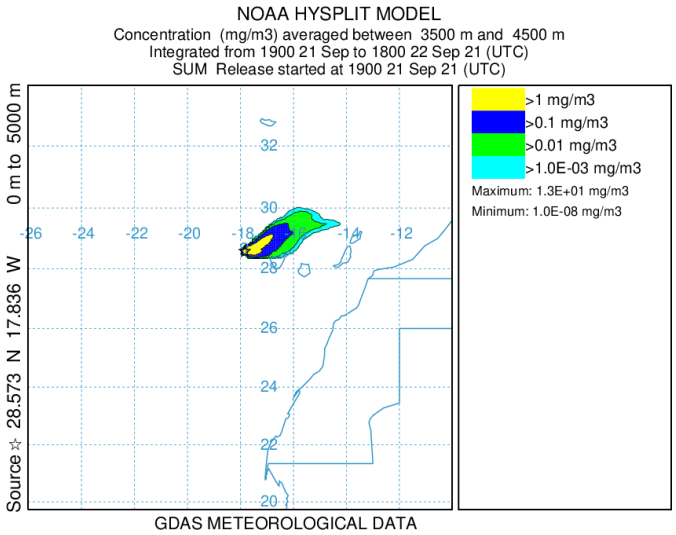

Figure 2: Dispersion of volcanic ash, continuously ejected from the Cumbre Vieja volcano one day before the LIDAR measurement, as obtained from the NOAA ARL HYSPLIT Dispersion Model [13, 14]. The colour contours represent the daily average of ash concentration at altitudes between 3500 m a.s.l. and 4500 m a.s.l. where the elevated aerosol layer was observed by the BRL. Numerical values of ash concentrations can be regarded as estimates only due to the quantitatively unknown volcanic mass ejection rate during that time.

3. Cumbre Vieja volcano plume observation

On 19 September 2021, the Cumbre Vieja volcano erupted in the southern part of the La Palma island. The volcano is located about 14 km air distance toward the south-south-east of the ORM. In the following days, the plume spread over the whole island, as shown in Fig. 2.

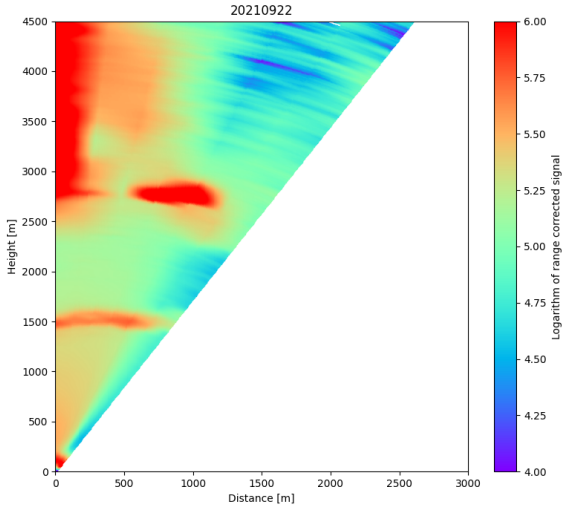

Figure 3: Spatial distribution of clouds and aerosol loading above the ORM on 22 September 2021. The plot is based on seven 90 s long measurements in the 355 nm return channel at different zenith angles ranging from 0° to 30° in steps of 5°. A barycentric interpolation was used to fill the gaps. The volcanic ash layer is clearly visible 1500 m above the observatory (approximately 3700 m a.s.l.).

During the measurements in the evening of 22 September 2021, a vertical scan of the sky was performed. At that time, the laser was not yet operated at full power, and the high voltages of the elastic-lines PMTs were reduced in order to protect the readout system after the reflectivity increase of the realuminized main mirror. Only later during spring 2022 further protective measures were introduced and the system was operated at full power. In the obtained data, two distinct features are visible: an optically thick layer of clouds at altitudes above 2300 m a.g.l. directly above the LIDAR, at a zenith angle of 0° (Fig. 3), which dissipates out toward the north, and a thinner layer located at an altitude of 1500 m a.g.l., which covers all the scanned sky quite homogeneously. From the ratio between the extinction and backscattering coefficients

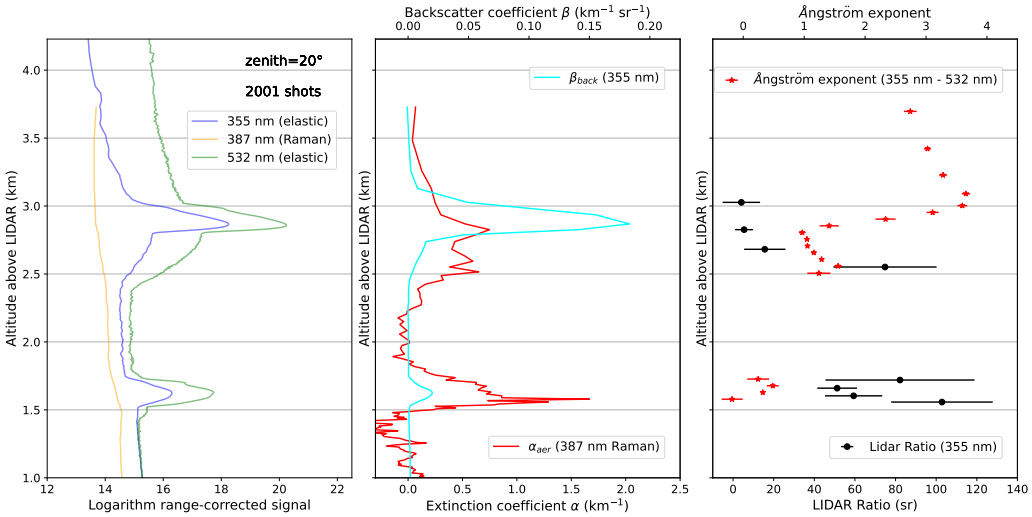

Figure 4: **Left:** Range square corrected LIDAR returns in the three analog channels, where blue at 355 nm and green at 532 nm are elastic and orange at 389 nm is the Raman backscattering channel. The measurement was performed at a zenith angle of 20° with 2001 laser shots at 10 Hz rate. **Center:** The backscattering coefficient retrieved from 355 nm channel in cyan and the extinction coefficient of aerosols retrieved from Raman 389 nm channel in red. The extinction coefficient exhibits same peaks. that are visible in backscattering channels, but in the case of extinction the lower peak is much more prominent. **Right:** Ångström exponent profile (355 nm-532 nm) in red stars and the LIDAR ratio for 355 nm channel in black dots.

at one wavelength, the so-called LIDAR ratio, shown in Fig. 4, we can further distinguish two layers: one with large diameter scatterers at about 1.6 km above the LIDAR, and another layer of much smaller particulates beyond 2.3 km a.g.l. Similar conclusions can be drawn from the ratio between the extinction coefficients of two different wavelengths, the so-called Ångström exponent. We obtained a LIDAR ratio of (76±20) sr and an Ångström exponent of 0.30±0.02 for the lower overdensity, indicative of particles with large diameters, while the LIDAR ratio for the upper one is considerably smaller and comparable with almost point-like scatterers. Note that a transition is visible within the upper layer from larger (below 2.8 km) to smaller scatterers. From the combined results of both ratios and knowledge about the local environment, we can conclude that the lower aerosol loading is composed of volcanic ash that was dispersed from the Cumbre Vieja volcano plume, while the upper part must be due to a cloud with typical characteristics for the La Palma atmosphere at those altitudes. This is also corroborated by satellite data, shown in Fig. 5. Even though, during the LIDAR measurement, the plume is found below the thick cloud layer, completely covering it from the satellite view, the clockwise motion of the plume visible in multiple consecutive satellite suggests that it was located above the ORM during the time of measurement.

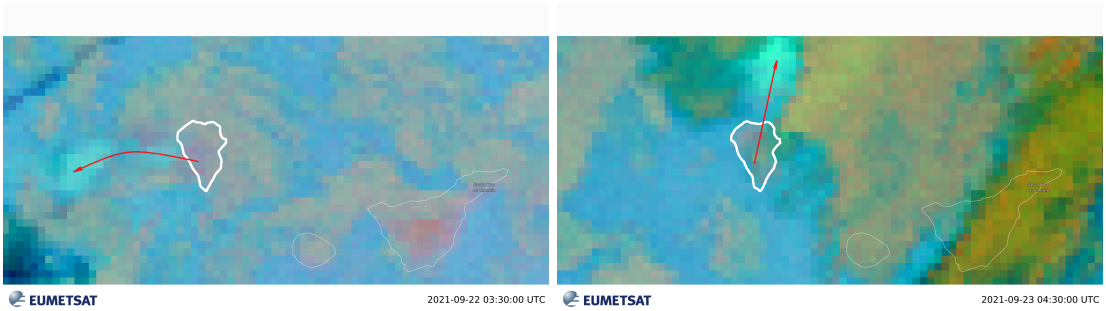

Figure 5: Satellite image (*Volcanic Ash RGB - MSG - 0 degree*) of the volcanic plume (cyan, corresponding to enhanced SO_2 concentration) above La Palma. The left image was taken on Sep. 22, 2021 at 03:00 UTC, our LIDAR measurement was performed at 19:30 UTC, and the right image was taken after the measurement, on Sep. 23, 2021 at 04:30 UTC. The wind direction (on the images indicated with red arrow) changed in a clockwise manner, which blew the plume above the observatory. ©EUMETSAT 2021.

4. Conclusion

The volcano eruption provided a possibility to test the device in a rare event, which allowed to check device performance in extreme conditions. Furthermore, it showed that the BRL can also work as meteorological LIDAR with capabilities of basic aerosol classification, although limited, as it was not primarily designed for this task.

Acknowledgements

We thank the LST-1 collaboration for the use of their experimental area at ORM. We also gratefully acknowledge the NOAA Air Resources Laboratory (ARL) for the provision of the HYSPLIT transport and dispersion model and/or READY website `https://www.ready.noaa.gov` used in this publication. Satellite images are ©EUMETSAT. This research was co-funded by the Slovenian Research Agency, grants P1-0031, I0-0033, J1-9146. The financial support of the Spanish grant PID2019-107847RB-C42, funded by MCIN/AEI/ 10.13039/501100011033 is gratefully acknowledged. MD acknowledges funding from Italian Ministry of Education, University and Research (MIUR) through the "Dipartimenti di eccellenza" project Science of the Universe".

References

[1] Rodriguez-Franco J J and Cuevas E 2013 *Journal of Geophysical Research: Atmospheres* **118** 10,754–10,769
[2] Munar-Adrover P and Gaug M 2019 *AtmoHEAD 2018, Anacapri* (*EPJ Web Conf.* vol 197) p 01002
[3] C Fruck M Gaug A H *et al.* 2022 *MNRAS* **stac1563** in press, arXiv:2202.09561
[4] Wang L *et al.* 2016 *Geophysical research abstracts* **18**
[5] Bernlöhr K 2000 *Astrop. Phys.* **12** 225
[6] Gaug M 2017 *AtmoHEAD 2016, Olomouc* (*EPJ Web Conf.* vol 144) p 01003
[7] Doro M *et al.* 2013 *AtmoHEAD Conference, Saclay* arXiv:1402.0638
[8] Ballester O *et al.* 2019 *PoS(ICRC2019)* **814**
[9] Gaug M *et al.* 2019 *AtmoHEAD 2018, Anacapri* (*EPJ Web Conf.* vol 197) p 02005
[10] Alexandreas D *et al.* 1995 *NIM* A **360** 385–389
[11] Baillon P *et al.* 1989 *NIM* A **276(3)** 492–495
[12] Baillon P *et al.* 1989 *NIM* A **277(2)** 338–346
[13] Stein A F *et al.* 2015 *Bull. Amer. Meteor. Soc.* **96** 2059–2077
[14] Rolph G *et al.* 2017 *Environmental Modelling & Software* **95** 210–228
[15] Da Deppo V *et al.* 2012 *Proc. SPIE Optical Systems Design* vol 8550 p 85501V
[16] Mazin D *et al.* 2021 *PoS (ICRC2021)* **872**